Nanoscale Res Lett (2010) 5:797–804
DOI 10.1007/s11671-010-9560-y

NANO EXPRESS

Luminescent Organic–Inorganic Hybrids of Functionalized Mesoporous Silica SBA-15 by Thio-Salicylidene Schiff Base

Ying Li · Bing Yan · Jin-Liang Liu

Received: 5 January 2010 / Accepted: 3 February 2010 / Published online: 19 February 2010

Abstract Novel organic–inorganic mesoporous luminescent hybrid material *N*,*N*′-bis(salicylidene)-thiocarbohydrazide (BSTC-SBA-15) has been obtained by co-condensation of tetraethyl orthosilicate and the organosilane in the presence of Pluronic P123 surfactant as a template. *N*,*N*′-bis(salicylidene)-thiocarbohydrazide (BSTC) grafted to the coupling agent 3-(triethoxysilyl)-propyl isocyanate (TESPIC) was used as the precursor for the preparation of mesoporous materials. In addition, for comparison, SBA-15 doped with organic ligand BSTC was also synthesized, denoted as BSTC/SBA-15. This organic–inorganic hybrid material was well-characterized by X-ray diffraction, Fourier transform infrared spectroscopy, transmission electron microscopy (HRTEM), and photoluminescence spectra, which reveals that they all have high surface area, uniformity in the mesostructure. The resulting materials (BSTC-SBA-15 and BSTC/SBA-15) exhibit regular uniform microstructures, and no phase separation happened for the organic and the inorganic compounds was covalently linked through Si–O bonds via a self-assemble process. Furthermore, the two materials have different luminescence range: BSTC/SBA-15 presents the strong dominant green luminescence, while BSTC-functionalized material BSTC-SBA-15 shows the dominant blue emission.

Keywords Organic–inorganic hybrid material · Functionalized mesoporous silica · Photoluminescence · Schiff-base derivative

Y. Li · B. Yan (✉) · J.-L. Liu
Department of Chemistry, Tongji University, Siping Road 1239, Shanghai 200092, China
e-mail: byan@tongji.edu.cn

Introduction

Organic–inorganic hybrid materials have been subjected to more intense development in the field of materials science since they not only combine the respective beneficial characters of organic and inorganic components but also often exhibit exceptional properties that exceed what would be excepted for a simple mixture of the components [1–4]. The hybrid materials enable both inorganic and organic dopants to be incorporated with relatively high thermal stability [5–7]. According to the chemical nature or different synergy between components, hybrids can be categorized into two main classes. Class I concerns all systems where no covalent bond is present between organic and inorganic parts but only weak interactions (such as hydrogen bonding, van der waals forces or electrostatic forces) exist between organic and inorganic moieties [8, 9]; the corresponding conventional doping methods seems hard to prohibit the problem of quenching effect on luminescent centers due to the high vibration energy of the surrounding hydroxyl groups. Class II materials belong to the molecular-based composite materials in which the organic and inorganic phases are linked together through strong chemical bonds (covalent, ion-covalent, or coordination bonds). Through the combination of chemical bonding within the different components in a single material, this kind of materials can realize the possibility of tailoring the complementary properties of both components to obtain novel multifunctional materials with attractive performances such as mechanical, thermal, and other physical and chemical properties [10–12]. As a result, a few studies in terms of the covalently bonded hybrids [13] have appeared and the as-derived molecular-based materials exhibit monophasic appearance [14–18], besides, the reinforcement of thermal and mechanical resistances has

been clearly established. Our research group is concentrated on covalently grafting the ligands to the inorganic networks in which organic groups are bonded with a siloxane matrix through Si–O linkage using different modified routes, including the modification of active amino group, hydroxyl groups, and carboxyl groups with coupling agent, etc [19–22].

Recently, organic-functionalized mesoporous siliceous materials have generated a great deal of interest in the fields of catalysis, adsorption [23–28], and sensors [29] due to their high surface areas and large ordered pores ranging from 2 to 50 nm with narrow size distributions. Mesoporous materials are a special type of nonmaterials with ordered arrays of uniform nanochannels. Among them, SBA-15 is by far the largest pore size mesochannels, with thick walls, adjustable pore size from 3 to 30 nm, and high hydrothermal and thermal stability [30–33]. These properties together with the thermal and mechanical stabilities make it as an ideal host for incorporation of active molecules, and some work has already been devoted on this field. The design and synthesis of innovative functionalized hybrid mesoporous materials are of considerable interest and open up an extraordinary field of investigation [34–36]. Many research efforts, which have focused on preparing the organic–inorganic hybrids through functionalization of the exterior and/or interior surfaces, prompted the utilization of mesoporous SBA-15 in many areas. However, the synthesis and luminescence properties of SBA-15 mesoporous materials covalently bonded with organic schiff-base ligands have hardly been explored to date [37]. Schiff-base compounds were reported to possess cytotoxic, anticonvulsant, antiproliferative, and anticancer activities; some Schiff-base ligands have potential applications in organic synthesis, catalysis, medicinal chemistry, and biotechnology.

Here, we report on the synthesis and characterization of *N*,*N*′-bis(salicylidene) –thiocarbohydrazide (BSTC) functionalized SBA-15 mesoporous hybrid material (denoted as BSTC-SBA-15), in which BSTC was covalently bonded to the framework of SBA-15 by co-condensation of the modified BSTC (denoted as BSTC-Si) and the tetraethoxysilane (TEOS) using the Pluronic P123 surfactant as template. N,N'-bis(salicylidene) –thiocarbohydrazide (BSTC) was first synthesized by the reaction of salicylaldehyde with thiocarbohydrazide. Because the organic compounds are covalently bonded to the silica network through Si–C bonds, the organic groups become an integral part of the materials and thus homogeneous complicated huge molecule systems with regular uniform microstructures were obtained. In addition, for comparison, SBA-15 doped with BSTC was also synthesized, denoted as BSTC/SBA-15. Full characterization and detail studies of luminescence properties of all these synthesized materials were investigated in relation to guest–host interactions between the organic complex and the silica matrix.

Experimental Section

Chemicals

Pluronic P123 ($EO_{20}PO_{70}EO_{20}$, Aldrich), Tetraethoxysilane (TEOS, Aldrich) was distilled and stored under nitrogen atmosphere and 3-(triethoxysiyl)-propyl isocyanate (TEPIC, Lancaster) was used. All the other reagents are analytically pure.

Synthetic Procedures

Synthesis of BSTC-Functionalized SBA-15 Mesoporous Material by Covalent Bond (Denoted as BSTC-SBA-15)

Synthesis of Thiocarbohydrazide Twenty microliter of 85% hydrazine hydrate was dissolved in 60 mL of water, and then 6 mL CS_2 was added dropwise, the reaction mixture was kept under room temperature for 1 h and then heated to 90°C for an additional 8 h. After cooling, the precipitate was filtered off, washed with water, and dried. The crude product was purified by recrystallization from water and finally obtained as white needles, yield 6.02 g (72%). m.p.172–173°C. ^{1}H NMR (DMSO): δ 4.48 (d, 4H, NH_2), 8.69 (t, 2H, NH).

Synthesis of SBA-15 SBA-15 host structure was synthesized according to the reported procedure using Pluronic P123 as a structure-directing agent and tetraethyl orthosilicate (TEOS) as a silica source under acidic conditions [38]. Typically, 1.0 g of P123 was dissolved in 7.5 g of H_2O and 30 g of dilute HCl solution (2.0 M) with stirring at 35°C. Then, 2.08 g of TEOS was added dropwise to the solution with stirring for 24 h and transferred into a Teflon bottle sealed in an autoclave, which was heated at 100°C for 24 h. The solid product was filtered, washed thoroughly with deionized water, and dried at 60°C. The as-synthesized material was calcined from room temperature to 550°C at a heating rate of 2–6°C/min for 5 h to remove the templates and obtained fine mesoporous SBA-15.

Synthesis of BSTC *N*,*N*′-bis(salicylidene)-thiocarbohydrazide (BSTC) was prepared as follows: 0.493 g (4.4 mmol) salicylaldehyde was dissolved in 20 mL of absolute ethanol, and then 2 mmol thiocarbohydrazide was dissolved in 10 mL of absolute ethanol was added dropwise. The resulting mixture was heated under reflux for 3 h. After cooling, the precipitate was filtered off. The crude product was purified by recrystallization from

absolute ethanol and finally obtained as white crystals. ^{1}H NMR ($CDC1_3$, 500 MHz): δ 2.60 (s, 2H, NH); 6.89, 6.96, 7.32, 7.70 (8H, Ar); 8.52 (s, 2H, *Ar*CH); 11.75 (s, 2H, OH). ^{13}C NMR ($CDC1_3$, 100 MHz): δ 157.2, 132.2, 127.5, 121.4, 118.8, 116.2 (Ar); 156.4 (*Ar*CH); 184.2 (C=S).

Synthesis of BSTC-Si A typical procedure for the preparation of the modified precursor BSTC-Si was as follows: *N*,*N*′-bis (salicylidene)-thiocarbohydrazide (BSTC) (1 mmol) was first dissolved in 20 mL of pyridine with stirring, and 3-(triethoxysilyl)-propyl isocyanate (TESPIC) (2.2 mmol) dissolved in 10 ml of pyridine was added dropwise with stirring; the mixture was warmed at 80°C for approximately 12 h in a covered flask at the nitrogen atmosphere. After isolation and purification, a yellow oil sample BSTC-Si was obtained. ^{1}H NMR ($CDC1_3$, 500 MHz): δ 0.58 (t, 4H, CH_2Si); 1.20 (t, 18H, CH_3CH_2); 1.65(m, 4H, $NHCH_2CH_2CH_2Si$);1.80 (m, 2H, $NCH_2CH_2CH_2N$); 3.18(m, 4H, $NHCH_2$); 3.65(q, 12H, $SiOCH_2$); 3.70 (t, 4H, NCH_2 CH_2); 6.75, 6.90, 7.30, 7.42 (8H, Ar); 8.01 (t, 2H,NH); 8.50 (s, 2H, *Ar*CH). ^{13}C NMR ($CDC1_3$, 100 MHz): δ 13.7 (CH_2Si); 18.4(CH_3CH_2O); 25.5 ($NHCH_2CH_2CH_2Si$); 31.6 ($NCH_2CH_2CH_2N$); 43.2 ($NHCH_2$); 56.8 (NCH_2CH_2); 58.4(CH_3CH_2O); 152.1, 131.2, 131.0, 130.3, 124.6, 119.7, (Ar); 155.4 (C=O), 157.5(*Ar*CH).

And then, the mesoporous material BSTC-SBA-15 was synthesized from acidic mixture with the following molar composition: 0.0172 P123: 0.96 TEOS: 0.04 BSTC-Si: 6 HCl: 208.33 H_2O. P123 (1.0 g) was dissolved in the deionized water (7.5 g) and 2 M HCl solution (30 g) at room temperature. A mixture of BSTC-Si and TEOS was added into the above-mentioned solution with stirring for 24 h and transferred into a Teflon bottle sealed in an autoclave, which was heated at 100°C for 48 h. The solid product was filtrated, washed thoroughly with deionized water, and dried at 60°C. Removal of copolymer surfactant P123 was conducted by Soxhlet extraction with ethanol under reflux for 2 days. The material was dried in a vacuum and showed a light-yellow color (Fig. 1).

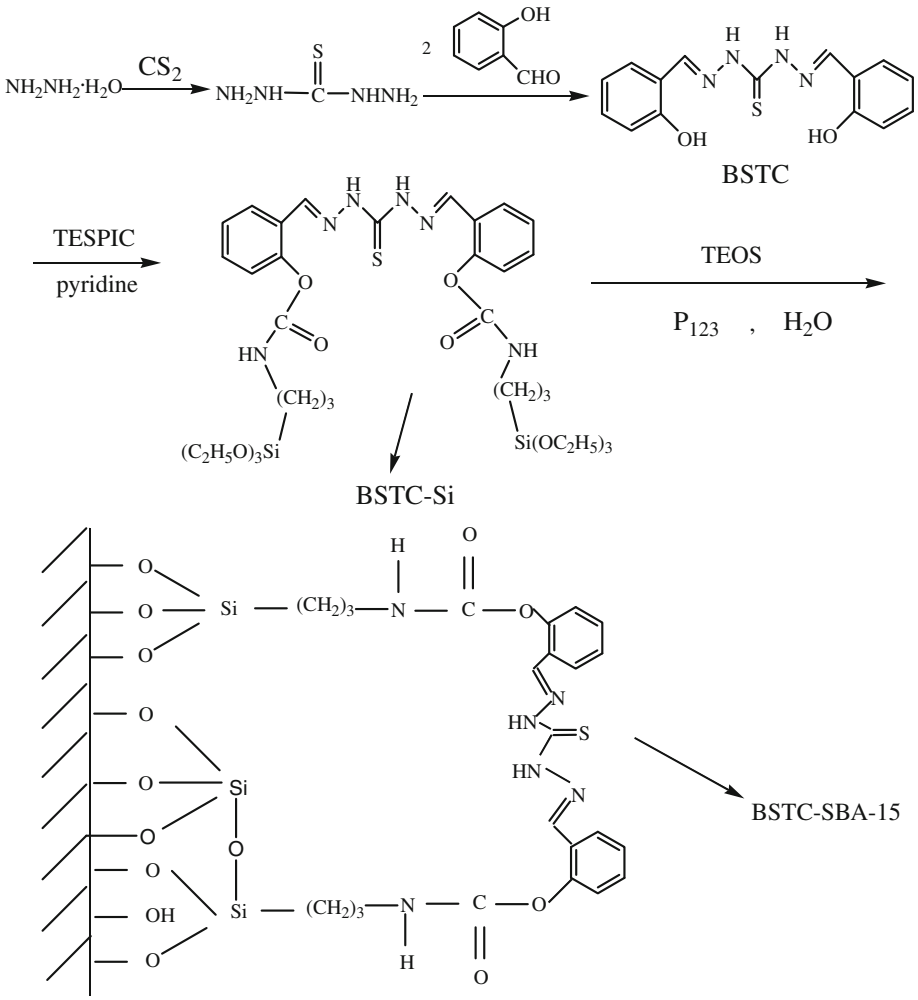

Fig. 1 Scheme of the synthesis process of BSTC–Si and predicted structure of hybrid mesoporous material BSTC-SBA-15

Synthesis of SBA-15 Doped With N,N′-bis (salicylidene)-thiocarbohydrazide (Denoted as BSTC/SBA-15)

The encapsulation method of the mesoporous silica SBA-15 doped with *N*,*N*′-bis (salicylidene)-thiocarbohydrazide (BSTC) in ethanol solution together with SBA-15. The mixture was stirred at room temperature for 12 h, and the resulting samples were filtered, washed with ethanol, dried at 60°C under vacuum overnight. The mesoporous materials were denoted as BSTC/SBA-15 (Fig. 1).

Characterization

IR spectra were measured within the 4,000–400 cm^{-1} region on an infrared spectrophotometer using the KBr pellet technique. ^{1}H NMR spectra were recorded in $CDCl_3$ on a Bruker AVANCE-500 spectrometer with tetramethylsilane (TMS) as internal reference. The ultraviolet absorption spectra were taken with an Agilent 8453 spectrophotometer. X-ray powder diffraction patterns were recorded on a Rigaku D/max-rB diffractometer equipped with a Cu anode in a 2θ range from 0.6° to 6°. Nitrogen adsorption/desorption isotherms were measured at the liquid nitrogen temperature, using a Nova 1000 analyzer. Surface areas were calculated by the Brunauer-Emmett-Teller (BET) method, and pore size distributions were evaluated from the desorption branches of the nitrogen isotherms using the Barrett-Joyner-Halenda (BJH) model. The fluorescence excitation and emission spectra were obtained on a Perkin-Elmer LS-55 spectrophotometer. Luminescence lifetime measurements were taken on an Edinburgh FLS920 phosphorimeter using a 450-w xenon lamp as excitation source. Transmission electron microscope (TEM) experiments were conducted on a JEOL2011 microscope operated at 200 kV or on a JEM-4000EX microscope operated at 400 kV.

Results and Discussion

As detailed in the experimental section, ^{1}H as well as ^{13}C spectra relative to BSTC, the silylated precursors, BSTC-Si, are in full agreement with the proposed structure. The ^{1}H NMR chemical shift relative to -OH bond can be observed in Schiff-base compound BSTC and is disappeared in the corresponding silylated precursor BSTC-Si, which indicates that the accomplishment of the hydrogen transfer reaction between OH and the TESPIC. Integration of the ^{1}H NMR and ^{13}C signals corresponding to ethoxy groups shows that no hydrolysis of the precursors occurred during the grafting reaction.

The presence of the organic ligand BSTC covalently bonded to the mesoporous SBA-15 was characterized by IR and UV absorption spectra. The IR spectra for thiocarbohydrazide (A), TESPIC (B), BSTC (C), BSTC-Si (D), and BSTC-functionalized hybrid mesoporous material BSTC-SBA-15 (E) are shown in Fig. 2. From C to D, the apparent characteristic absorption peak at 3272, 3203 of amino groups cannot be observed in BSTC. Together with the emergence of the strong vibrations bonds of C=N at 1,620 cm^{-1} proves the formation of the Schiff-base compound BSTC. Furthermore, in Fig. 2(D), the grafting reactions of TESPIS with BSTC were supported by the bands located at 1,642 cm^{-1}, which originated from the absorption of amide groups (–CONH–). In addition, the bending vibration (δ_{NH}, 1,563 cm^{-1}) further proves the formation of amide groups. Otherwise, the presence of a series of strong bands at around 2,974, 2927, 2,887 cm^{-1} due to the vibrations of methylene $-(CH_2)_3-$ and the disappearance of the stretch vibration of the absorption peaks at 2,250–2,275 cm^{-1} for N=C=O of TESPIC indicate that TESPIC has been successfully grafted on to the BSTC. Furthermore, the spectrum of BSTC-Si is dominated by ν(C–Si, 1,196 cm^{-1}) and ν (Si–O, 1,070 cm^{-1}) absorption bands, characteristic of trialkoxylsilyl functions. In panel E of Fig. 2, the formation of the Si–O–Si framework is evidenced by the bands located at 1,088 cm^{-1} (ν_{as}, Si–O), 813 cm^{-1} (ν_s, Si–O), and 466 cm^{-1} (δ, Si–O–Si) (ν represents stretching, δ in plane bending, s symmetric, and as asymmetric vibrations). Furthermore, the peaks at 1,631 and 1,550 cm^{-1} originating from –CONH– group of BSTC-Si can also be observed in hybrid mesoporous material BSTC-SBA-15 (E), which is consistent with the fact that the BSTC group in the framework remains intact after both hydrolysis/condensation reaction and the surfactant extraction procedure [38].

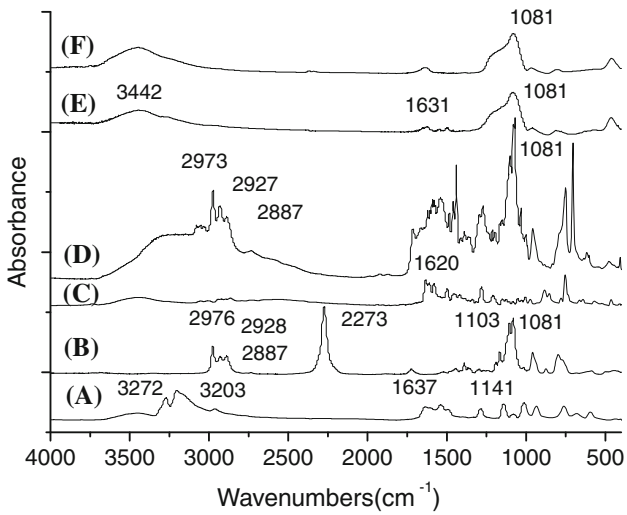

Fig. 2 IR spectra for thiocarbohydrazide (*A*), TESPIC (*B*), BSTC (*C*), BSTC-Si (*D*), BSTC-functionalized hybrid mesoporous material BSTC-SBA-15 (*E*), and pure SBA-15 (*F*)

The maximal ultraviolet absorption wavelengths of Schiff-base BSTC and the corresponding silylated precursor BSTC-Si are shown in Table 1. As for BSTC, the maximal absorptions are located at 303 and 340 nm, which attributed to the $\pi \rightarrow \pi^*$ transition of the aromatic and the C=N groups. Compared with the Schiff-base compound BSTC, there was only a small shift occurred in the corresponding silylated precursor BSTC-Si. This is due to that the conjugating effect was nearly not alter after grafting to the TESPIC so the energy difference levels among the $\pi \rightarrow \pi^*$ transition were not changed.

The small-angle X-ray diffraction (SAXRD) patterns and nitrogen adsorption/desorption isotherms are popular and efficient methods to characterize highly ordered mesoporous material with hexagonal symmetry of the space group *p6mm*. The SAXRD patterns of pure SBA-15 mesoporous silica (A), BSTC-SBA-15 (B), BSTC/SBA-15 (C) are presented in Fig. 3. All the materials exhibit three well-resolved diffraction peaks that can be indexed as (100), (110), and (200) reflections associated with 2-D hexagonal symmetry (*p6mm*), confirming a well-ordered mesoporous structure in these samples. Compared with the SAXRD pattern of pure SBA-15, the d_{100} spacing values of BSTC-SBA-15 and BSTC/SBA-15 are nearly unchanged (see Table 2), indicating that the ordered hexagonal mesoporous structure of SBA-15 retains intact after the introduction of organic group. However, it is worth noting that the intensity of these characteristic diffraction peaks decreases slightly in the BSTC-functionalized mesoporous materials when compared with pure SBA-15, which is probably due to the presence of guest moieties onto the mesoporous framework of SBA-15, resulting in the decrease in crystallinity, but not the collapse in the pore structure of mesoporous materials [39].

The N_2 adsorption/desorption isotherm (top plot) and the pore size distribution (bottom plot) for pure SBA-15(A), BSTC-SBA-15 (B), BSTC/SBA-15 (C) samples are shown in Fig. 4. They all display type IV isotherms with H1-type hysteresis loops at high relative pressure according to the IUPAC classification [40–42], characteristic of mesoporous materials with highly uniform size distributions. From the two branches of adsorption/desorption isotherms, the presence of a sharp adsorption step in the P/P_0 region from 0.6 to 0.8 and a hysteresis loop at the relative pressure $P/P_0 > 0.7$ show that the materials process a well-defined array of regular mesopores. The specific area and the pore size have been calculated by using

Table 1 The maximal ultraviolet absorption wavelengths of BSTC

Compounds	BSTC	BSTC-Si
λ_{max} (nm)	303, 340	312, 346

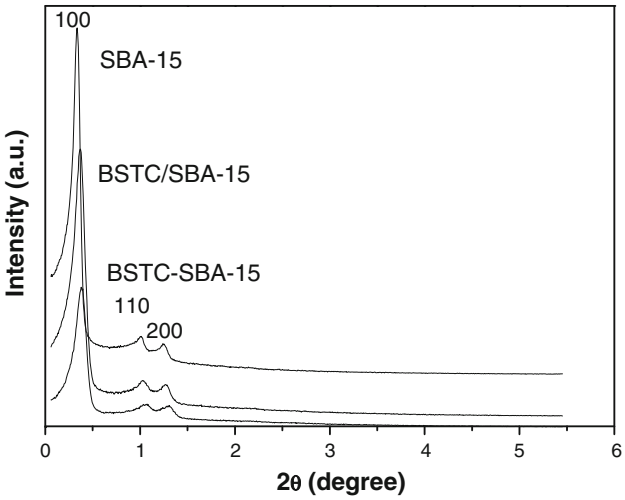

Fig. 3 AXRD patterns of SBA-15, BSTC/SBA-15, and BSTC-SBA-15

Table 2 Textural data of SBA-15, BSTC/SBA-15 and BSTC-SBA-15

Sample	d_{100} (nm)	S_{BET} (m^2/g)	V(cm^3/g)	D_{BJH} (nm)
SBA-15	10.68	746	0.97	5.64
BSTC/SBA-15	10.15	551	0.76	5.24
BSTC-SBA-15	10.12	624	0.84	5.40

d_{100} is the d(100) spacing, S_{BET}-the BET surface area, V-the pore volume, and D-the pore diameter

Brunauer-Emmett-Teller (BET) and Barrett-Joyner-Halenda (BJH) methods, respectively. And the structure data of all these mesoporous materials (BET surface area, total pore volume, and pore size, etc.,) were summarized in Table 2. It is known that calcined SBA-15 has a high BET surface area (746 m^2/g), a large pore volume (0.97 cm^3/g), and pore size (5.64 nm), indicative of its potential application as a host in luminescence materials. After functionalized with BSTC through covalent bond, the BSTC-SBA-15 exhibits a smaller specific area and a slightly smaller pore size and pore volume in comparison with those of pure SBA-15, which might be due to the presence of organic ligand BSTC on the pore surface and the co-surfactant effect of BSTC-Si, which interacts with surfactant and reduces the diameter of the micelles [43].

From the HRTEM images (as shown in Fig. 5) of BSTC-SBA-15, we could find that the ordered pore structure was still substantially conserved after the complexation. It confirms the suggested *p6mm* symmetry and a well-ordered hexagonal structure, which is also in agreement with the SAXRD and N_2 adsorption/desorption isotherms. The distance between the centers of the mesopore is estimated to be 10 nm, in good agreement with the value determined from the corresponding XRD data (see Table 2).

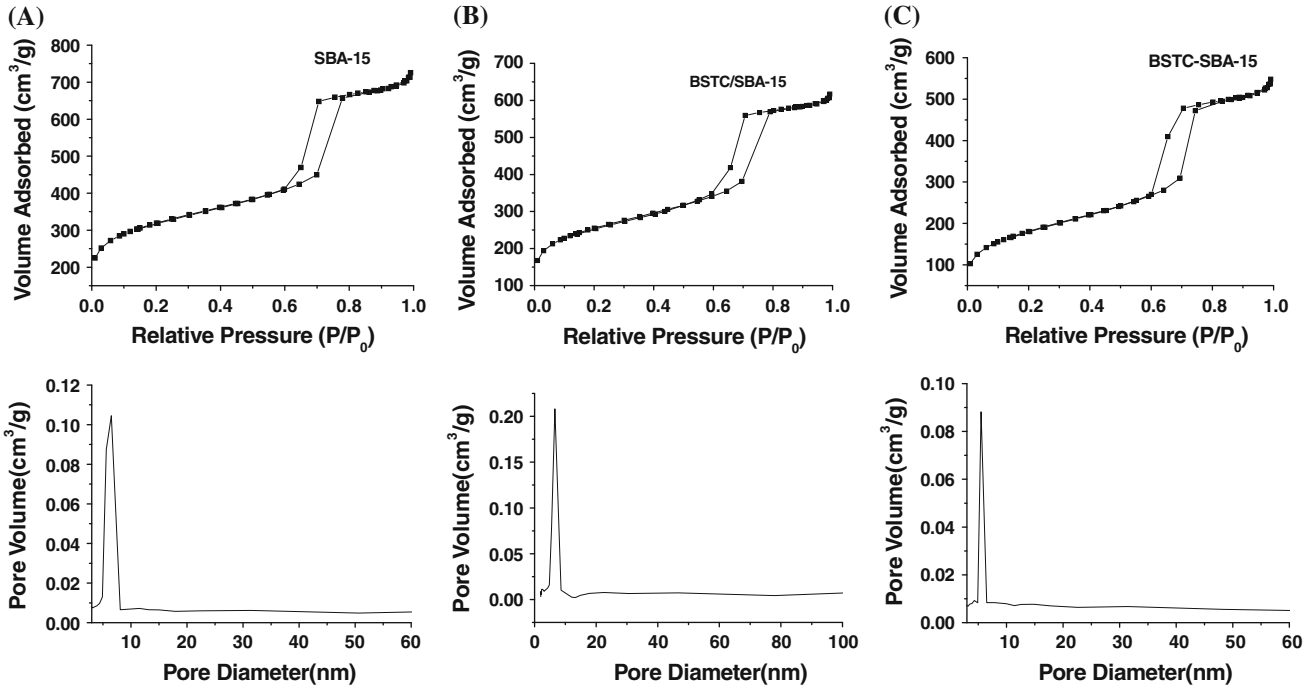

Fig. 4 N_2 **ad**sorption/desorption isotherms (*top*) and the pore diameter distributions (*bottom*) of pure SBA-15 (**a**), BSTC/SBA-15 (**b**) and BSTC-SBA-15 (**c**)

Figure 6 shows the excitation (a) and emission (b) spectra of BSTC ($\lambda_{em} = 537$ nm, $\lambda_{ex} = 396$ nm), BSTC/SBA-15($\lambda_{em} = 540$ nm, $\lambda_{ex} = 396$ nm), BSTC-SBA-15($\lambda_{em} = 467$ nm, $\lambda_{ex} = 354$ nm), and pure SBA-15($\lambda_{em} = 460$ nm, $\lambda_{ex} = 352$ nm). The excitation spectrum presents a large broad band from 350 to 410 nm in BSTC and BSTC/SBA-15, respectively. The broad band is attributed to the light absorption by the organic ligand. From the spectra, we can see that BSTC and BSTC/SBA-15 have the similar maximum excitation wavelengths which are located at 396 nm, while the excitation wavelength of the material BSTC-SBA-15 is around 354 nm, which is smaller than that of BSTC and BSTC doped material BSTC/SBA-15. The blue shift of the excitation bands as the introduction of organic group into the mesoporous material SBA-15 through covalent bond is due to a hypsochromic effect resulting from the change in the polarity of the environment surrounding the organic group in the mesoporous material [44]. The same difference can also be seen in the emission spectra. From the emission spectra of all the materials, it can be clearly seen that mainly large broad bands from 450 to 545 nm in BSTC and BSTC/SBA-15. Both BSTC and BSTC/SBA-15 present the strong dominant green luminescence, while the BSTC-functionalized material BSTC-SBA-15 shows the dominant blue emission, mainly originated from the host matrix SBA-15. It is presumed that different structures in the mesoporous materials will induce to the different energy absorption and the different fluorescence emission. For this kind of materials show an excellent emission in blue or green range, they can be used as potential blue or green optical materials.

Quantum yields (η) were determined using a standard integrating sphere (diameter 6 cm) [45]. Optical path length of the cell was 5 mm. Corrected intensity functions of the excitation ($I_{ex}(\lambda_{ref})$ were determined by the excitation spectra of the system ($g_{ref}(\lambda)$: 450–480 nm, scan rate 60 nm/min)

$$I_{ex}(\lambda_{ref}) = \frac{\Phi}{\int g_{ref}(\lambda_{ref})} g_{ref}(\lambda). \quad (1)$$

Here, Φ is light intensities of excitation. Corrected intensity functions of light absorption with sample, I_{ex} (λ_{sam}), were also determined from excitation spectra of the system (450–480 nm, scan rate 60 nm/min), whereas the corrected intensity function of the emission was determined from emission spectra (I_{em} (λ), 550–800 nm, scan rate 60 nm/min).Quantum yield (η) was calculated from the equation as follows [45, 46]:

$$\eta = \frac{E_{emission}}{E_{absorption}} = \frac{\int \frac{\lambda}{hc} I_{em}(\lambda) d\lambda}{\int \frac{\lambda}{hc} \{I_{ex}(\lambda_{ref}) - I_{ex}(\lambda_{sam})\} d\lambda}. \quad (2)$$

On the basis of the earlier discussion, the quantum efficiencies of the mesoporous hybrid materials can be determined. Quantum yields of BSTC and BSTC/SBA-15 (Ex at 396 nm, 300–450 nm, emission quantum yield are 0.64% and 0.57%, respectively) and the material BSTC-

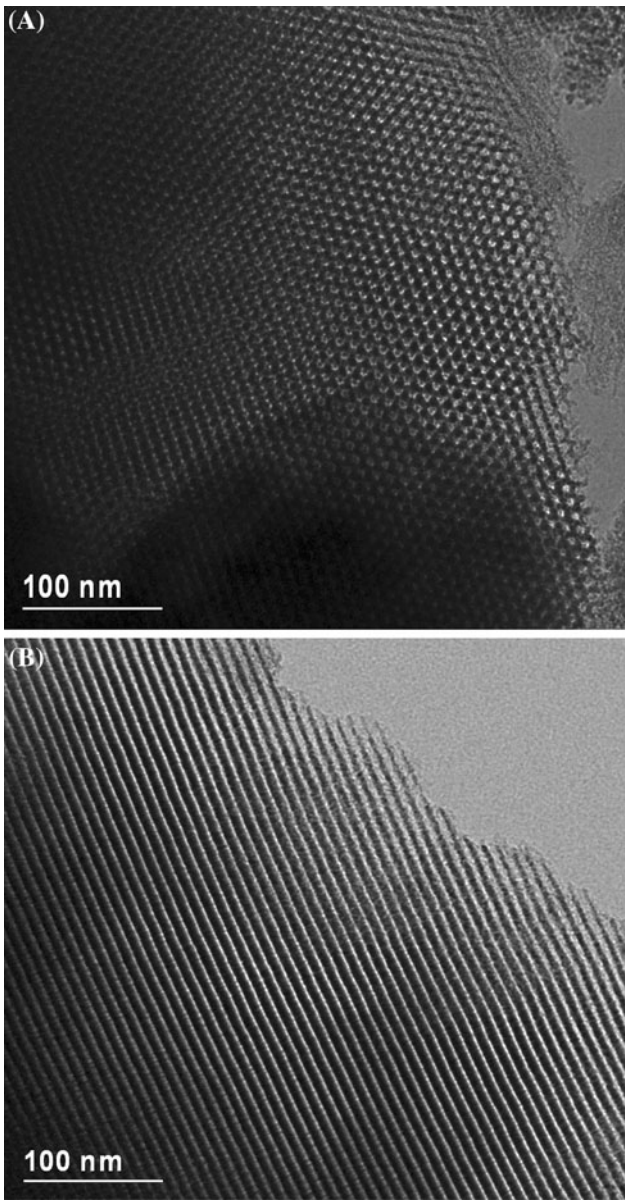

Fig. 5 HRTEM images of BSTC-SBA-15 recorded along the [100] (**a**) and [110] (**b**) zone axes

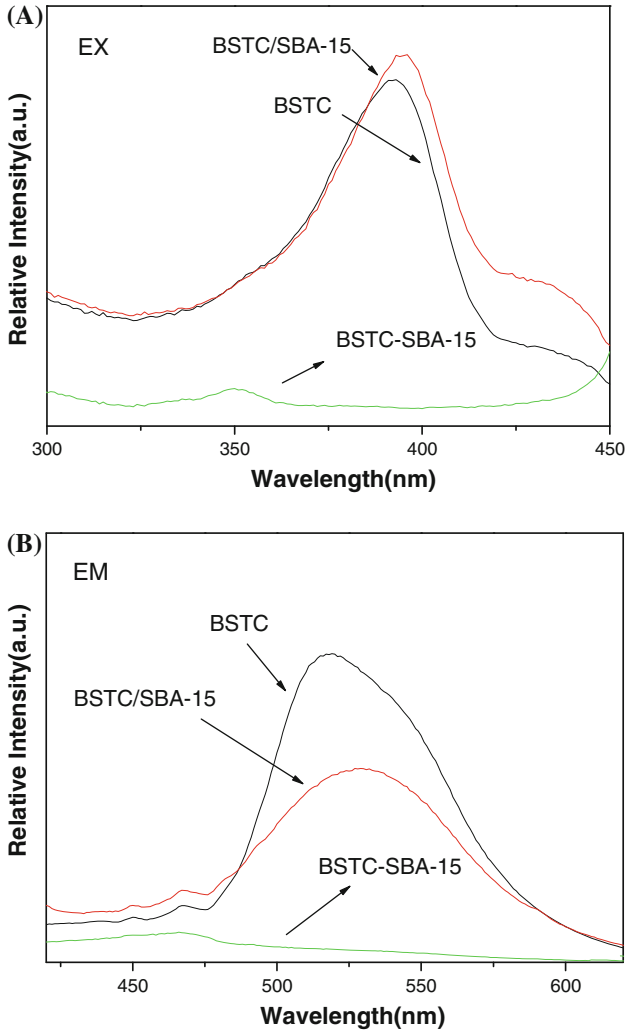

Fig. 6 The excitation (**a**) and emission spectra (**b**) for BSTC (λ_{em} = 537 nm, λ_{ex} = 396 nm), BSTC/SBA-15 (λ_{em} = 540 nm, λ_{ex} = 396 nm), BSTC-SBA-15(λ_{em} = 467 nm, λ_{ex} = 354 nm), and pure SBA-15(λ_{em} = 467 nm, λ_{ex} = 354 nm)

SBA-15 (Ex at 354 nm, 500–750 nm, emission quantum yield is 0.53%).

Conclusion

In summary, the organic Schiff-base has been successfully covalently immobilized in the ordered SBA-15 mesoporous material by the modification of *N*,*N*′-bis(salicylidene)–thiocarb-ohydrazide (BSTC) with 3-(triethoxysilyl)-propyl isocyanate (TESPIC) using a co-condensation method. New inorganic–organic hybrid mesoporous SBA-15-type material has been synthesized by co-condensation of TEOS and chelate ligand in the presence of P123 template. The synthesis of BSTC-SBA-15 provides a convenient approach of tailoring the surface properties of mesoporous silicates by organic functionalization, and the resulting materials all retain the ordered mesoporous structures. Further investigation into the luminescence properties of the mesoporous hybrids shows that all of the hybrids exhibit an excellent ability to absorb energy in ultraviolet–visible extent and have strong fluorescence emission intensities in blue or green range. This method allows the introduction of organic fluorophore with the preservation of uniform mesoscale channels, high specific, surface areas, and large pore volumes. As the synthesis process can be easily applied to other organic ligands and to different alkoxysilanes, we may expect to obtain stable and luminescent efficient hybrid materials in optical or catalysis areas.

Acknowledgments This work was supported by the National Natural Science Foundation of China (20971100) and Program for New Century Excellent Talents in University (NCET-08-0398).

References

1. P.G. Romero, Adv. Mater. **13**, 163 (2001)
2. J. Wen, G.L. Wilkes, Chem. Mater. **8**, 1667 (1996)
3. C. Guizard, P. Lacan, New J. Chem. **18**, 1097 (1994)
4. C. Sanchez, F. Ribot, New J. Chem. **18**, 989 (1994)
5. Q.A. Serra, I.L.V. Rosa, C.L. Medeiros, M.E.D. Zaniquell, J. Lumin. **112**, 60–61 (1994)
6. C. Sanchez, G.J. de A.A. Soler-Illia, F. Ribot, T. Lalot, C.R. Mayer, V. Cabuil, Chem. Mater. **13**, 3061 (2001)
7. R. Hernandez, A.C. Franville, P. Minoofar, B. Dunn, J.I. Zink, J. Am. Chem. Soc. **123**, 1248 (2001)
8. P.A. Tanner, B. Yan, H.J. Zhang, J. Mater. Sci. **35**, 4325 (2000)
9. N.I. Koslova, B. Viana, C. Sanchez, J. Mater. Chem. **3**, 111 (1993)
10. A.C. Franville, D. Zambon, R. Mahiou, Chem. Mater. **12**, 428 (2000)
11. F.Y. Liu, L.S. Fu, H.J. Zhang, New J. Chem. **27**, 233 (2003)
12. M. Schneider, K. Muller, Chem. Mater. **12**, 352 (2000)
13. H.R. Li, J. Lin, H.J. Zhang, L.S. Fu, Chem. Mater. **14**, 3651 (2002)
14. D.W. Dong, S.C. Jiang, Y.F. Men, X.L. Ji, B.Z. Jiang, Adv. Mater. **12**, 646 (2000)
15. H.R. Li, L.S. Fu, H.J. Zhang, Thin Solid Films **416**, 197 (2002)
16. H.R. Li, J. Lin, L.S. Fu, J.F. Guo, Q.G. Meng, F.Y. Liu, H.J. Zhang, Micropor. Mesopor. Mater. **55**, 103 (2002)
17. F.Y. Liu, L.S. Fu, J. Wang, Z. Liu, H.R. Li, H.J. Zhang, Thin Solid Films **419**, 178 (2002)
18. K. Binnemans, P. Lenaerts, K. Driesen, C. Gorller-Walrand, J. Mater. Chem. **14**, 291 (2004)
19. B. Yan, X.F. Qiao, J. Phys. Chem. B **111**, 12362 (2007)
20. Q.M. Wang, B. Yan, Cryst. Growth Des. **5**, 497 (2005)
21. Q.M. Wang, B. Yan, J. Photochem. Photobiol. A Chem. **177**, 1 (2006)
22. B. Yan, F.F. Wang, J. Organomet. Chem. **692**, 2395 (2007)
23. B. Lee, Y. Kim, H. Lee, J. Yi, Micropor. Mesopor. Mater. **50**, 77 (2001)
24. K. Liu, K. Hidajat, S. Kawi, D.Y. Zhao, Chem. Commun. (2000) 1145
25. K.Z. Hossain, L. Mercier, Adv. Mater. **14**, 1053 (2002)
26. H. Lee, J. Yi, Sep. Sci. Technol. **36**, 2433 (2001)
27. M.H. Lim, A. Stein, Chem. Mater. **11**, 3285 (1999)
28. K.Y. Ho, G. Mckay, K.L. Yeung, Langmuir **19**, 3019 (2003)
29. H.S. Zhou, H. Sasabe, I. Honma, J. Mater. Chem. **8**, 515 (1998)
30. D.Y. Zhao, J.P. Feng, Q.S. Huo, N. Melosh, G.H. Fredrickson, B.F. Chmelka, G.D. Stucky, Science **279**, 348 (1998)
31. D.Y. Zhao, J.Y. Sun, Q.Z. Li, G.D. Stucky, Chem. Mater. **12**, 275 (2000)
32. B.L. Newalkar, S. Komarneni, H. Katsuki, Chem. Commun. (2000) 2389
33. S. Madhugiri, A. Dalton, J. Gutierrez, J.P. Ferraris, K.J. Balkus, J. Am. Chem. Soc. **125**, 14531 (2003)
34. T. Hirano, K. Kikuchi, Y. Urano, T. Higuchi, T. Nagano, Angew. Chem. Int. Ed. **39**, 1052 (2000)
35. M.S. Panchard, R. Huber, M. Renault, H. Maas, R. Pansu, G. Calzaferri, Angew. Chem. Int. Ed. **40**, 2839 (2001)
36. Y. Li, B. Yan, Nanoscale Res. Lett. doi:10.1007/s11671-010-9534-0
37. Y. Li, B. Yan, Solid State Sci. **11**, 994 (2009)
38. D.Y. Zhao, Q.S. Huo, J.L. Feng, B.F. Chmelka, G.D. Stucky, J. Am. Chem. Soc. **120**, 6024 (1998)
39. Y. Li, B. Yan, H. Yang, J. Phys. Chem. C **112**, 3959 (2008)
40. K.S.W. Sing, D.H. Everett, R.A.W. Haul, L. Moscou, R.A. Pierotti, J. Rouquerol, T. Siemieniewska, Pure Appl. Chem. **57**, 603 (1985)
41. M. Kruk, M. Jaroniec, Chem. Mater. **13**, 3169 (2001)
42. W.H. Zhang, X.B. Lu, J.H. Xiu, Z.L. Hua, L.X. Zhang, M. Robertson, J.L. Shi, D.S. Yan, J.D. Holmes, Adv. Funct. Mater. **14**, 544 (2004)
43. C.Y. Peng, H.J. Zhang, Q.G. Meng, H.R. Li, J.B. Yu, F.J. Guo, L.N. Sun, Inorg. Chem. Commun. **8**, 440 (2005)
44. Q.G. Meng, P. Boutinaud, A.C. Franville, H.J. Zhang, R. Mahiou, Microp. Mesop. Mater. **65**, 127 (2003)
45. Y. Hasegawa, K. Sogabe, Y. Wada, T. Kitamura, N. Nakashima, S. Yanagida, Chem. Lett. (1999) 35
46. Y. Hasegawa, M. Yamamuro, Y.J. Wada, N. Kanehisa, Y. Kai, S. Yanagida, J. Phys. Chem. A **107**, 1697 (2003)